Received: 7 November 2022 | Revised: 19 May 2023 | Accepted: 26 May 2023

IET Computer Vision

DOI: 10.1049/cvi2.12212

The Institution of Engineering and Technology WILEY

ORIGINAL RESEARCH

A monocular image depth estimation method based on weighted fusion and point-wise convolution

Chen Lei[1] | Liang Zhengyou[1,2] | Sun Yu[1]

[1]School of Computer and Electronics Information, Guangxi University, Nanning, China

[2]Guangxi Key Laboratory of Multimedia Communications and Network Technology, Nanning, China

Correspondence

Liang Zhengyou, No. 100, University East Road, Nanning, Guangxi, China.
Email: zhyliang@gxu.edu.cn

Funding information

National Natural Science Foundation of China, Grant/Award Number: 61763002

Abstract

The existing monocular depth estimation methods based on deep learning have difficulty in estimating the depth near the edges of the objects in an image when the depth distance between these objects changes abruptly and decline in accuracy when an image has more noises. Furthermore, these methods consume more hardware resources because they have huge network parameters. To solve these problems, this paper proposes a depth estimation method based on weighted fusion and point-wise convolution. The authors design a maximum-average adaptive pooling weighted fusion module (MAWF) that fuses global features and local features and a continuous point-wise convolution module for processing the fused features derived from the (MAWF) module. The two modules work closely together for three times to perform weighted fusion and point-wise convolution of features of multi-scale from the encoder output, which can better decode the depth information of a scene. Experimental results show that our method achieves state-of-the-art performance on the KITTI dataset with $\boldsymbol{\delta}_1$ up to 0.996 and the root mean square error metric down to 8% and has demonstrated the strong generalisation and robustness.

KEYWORDS

computer vision, convolutional neural nets, estimation theory, image processing, indoor environment

1 | INTRODUCTION

Monocular cameras have the advantages of low price, rich content of acquired colour images and small size. One of the important research directions is to use the colour images acquired by monocular cameras to estimate depth information.

The use of deep learning techniques for depth estimation of monocular images has become a hot research topic in recent years. The unsupervised learning-based depth estimation of monocular images usually requires the combination of camera parameters and optical flow information for joint estimation [1, 2], which leads to large model parameters and difficult training. Monocular image depth estimation based on supervised learning [3–5] has some problems, such as insensitivity to object boundaries, weak textures and susceptibility to external factors such as light intensity, which makes it difficult to obtain a higher quality depth image. By constructing connected paths between multi-scale local features and global decoding streams by using the selected features of global and local features of the network, works [6] obtained higher quality depth images and improved the accuracy of depth estimation. The advantage of the model designed in this way is that the number of parameters is smaller, but the encoder layer is deeper while the decoder is shallower, which leads to insufficient decoding of the depth information of some scenes, thereby resulting in vagueness in estimating the boundary contours of the objects inside a complex scene.

In order to further improve the accuracy of depth estimation and obtain clear information of scene boundary, this paper proposes a new feature fusion module called maximum-average pooling weighted of feature fusion (MAWF). In this module, we use maximum pooling weighted and mean pooling weighted to fuse local features and global features respectively and finally average the two results. Using MAWF instead of channel concat allows features with significant channels to be weighted heavily and features with non-significant channels to

be weighted less. We also propose a continuous point-wise convolution module (CPCM) to reduce the dimensionality of the features after fusing global and local features. The CPCM module deepens the number of layers in the decoder of the network, which can better decode the feature information at multi-scale. Our method can efficiently restore the object boundary information and depth information of the scene, improve the model generalisation capacity and reduce the number of parameters in the network model. We have conducted extensive experiments on the NYU Depth V2 dataset [7] and KITTI dataset [8], and our experiments show that we have achieved good depth accuracy and boundary prediction accuracy.

The main contributions of this paper can be summarised as follows.

1. Designing a maximum-average pooling weighted fusion method to weight the features of different contributions to the depth estimation of a scene. The method can improve the accuracy of depth information and boundary information.
2. Designing and repeating the point-wise convolution module to reduce the fusion dimensionality of the global and local features. The module can reduce the number of parameters and deepen the understanding of features at multi-scale.
3. Extensive experiments on the NYU Depth V2 dataset and KITTI dataset prove the effectiveness of the proposed method. The method achieves state-of-the-art performance on the KITTI dataset and better robustness than the existing methods.

2 | RELATED WORD

Unsupervised learning has been extensively studied in the field of depth estimation. The authors in Ref. [1, 2] obtained sequential images by the movement of a monocular camera and used unlabelled monocular image sequences to implement the training of monocular depth networks and camera pose estimation networks. They combine the information of depth, camera motion and optical flow for joint estimation, which leads to the problems of large model parameters, difficult model design and high complexity of the algorithm.

Compared with the monocular depth estimation method of unsupervised learning, the depth estimation accuracy of the supervised learning method is greatly improved. In literatures [3–5, 9],three errors of measurement depth, gradient and surface normal are proposed as loss functions; they improve the accuracy of depth information estimation in a complementary way. Hu et al. [5] proposed an improved network architecture including encoder, decoder, multi-scale feature fusion module and refinement module. This method has the problems of low accuracy of depth estimation and inaccurate estimation of boundary information. Among them, the literature [9] proposed a boundary induction and scene aggregation network based on the work of Ref. [5], which solved the problem of 3D structure distortion of predicted depth information, the difficulty of estimating depth information near the edges and improved the boundary accuracy of predicted depth. However, the method designs multiple modules, and this leads to a huge number of model parameters, which is not conducive to practical applications. Kim et al [6] build the connection path between multi-scale local features and global decoding stream to generate a precisely estimated depth map. However, the encoder layer is deep, while the decoder is shallow, which leads to insufficient decoding of depth information of some scenes. Works in Refs. [10–15] are also based on the encoder-decoder structure, using multiple loss functions to improve the accuracy of depth information estimation in a complementary way. The depth estimation accuracy of these methods is often not high, and the model parameters are huge. The authors in Ref. [16] proved the importance of the high-order 3D geometric constraints for depth prediction. By designing a loss term that enforces a simple geometric constraint, namely, virtual normal directions determined by randomly sampled three points in the reconstructed 3D space, the accuracy and robustness of monocular depth estimation are significantly improved. Bhat et al. [17]divided the depth value into different intervals and applied the classification task to depth estimation. Ref. [18] needs additional data sets to participate in training and increase the difficulty of training. The authors in Ref. [19] use the encoder composed of the Transformer [20] branch and CNN branch to fully obtain long-distance correlation and local information, and multi-branch encoder leads to the complex model. The work in Ref. [21] introduces a spacing-increasing discretisation (SID) strategy to discretise depth and recast depth network; the methods in Refs. [17, 21] have complex data processing problems. The main contribution of literature [22] is to reconstruct the occluded part of the estimated depth information, and the depth estimation accuracy is not ideal. The authors in Ref. [23] proposed a local plane guidance layer to output plane coefficients and used it for full resolution depth estimation.

To sum up, the existing model methods have the disadvantages of inaccurate depth information prediction, insufficient depth estimation ability of images with more noise, low prediction accuracy of scene object boundaries or places with weak texture, large network parameters and high hardware resources consumption.

3 | METHODOLOGY

The depth estimation model in this study aims to predict the depth map $D \in R^{1\times w\times h}$ for a given RGB image $I \in R^{3\times w\times h}$. Our depth estimation model is composed of an encoder and a decoder, as shown in Figure 1. In particular, our encoders are from the SegFormer model [24]. SegFormer is a global-local path network, and it constructs global-local dependencies through the features of the decoder jump connection encoder.

Encoder: The input image I is processed with Embedding Patch [25] to obtain the features f_0, then, f_0 is fed into the first

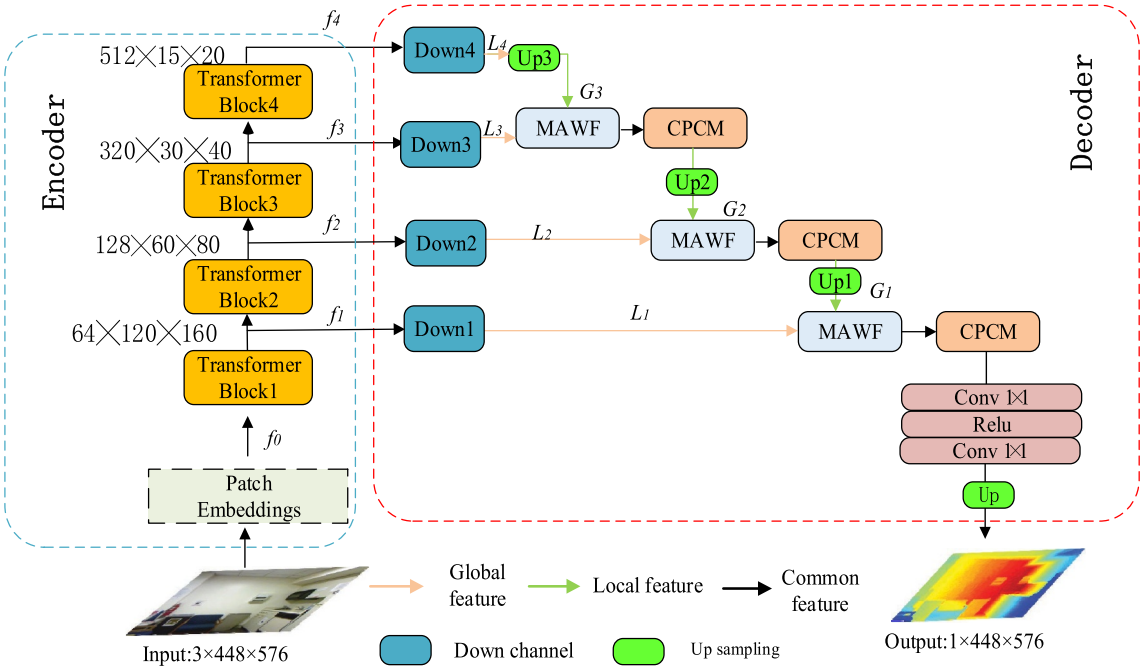

FIGURE 1 Network structure of the method in this study.

Transformer module to obtain the feature f_1, the features f_2, f_3, and f_4 are processed by the corresponding Transformer modules in turn. f_1, f_2, f_3 and f_4 corresponding to one-fourth, one-eighth, 1/16 and 1/32 of the input image size, and the channels are 64, 128, 320 and 512, respectively.

Decoder: Firstly, encoder output features, f_1, f_2, f_3 and f_4, are reduced to 64 channels by using 1×1 convolution kernel that obtains the local features L_1, L_2, L_3, $\overline{L}_4$. Secondly, the features of different sizes output from the encoder are weighted and convolved point-wise using three time by MAWF and CPCM, as shown in Figure 2, feature $\overline{L}_i$ is up-sampled to get G_{i-1} which has the same size as L_{i-1}. The process can be expressed as $G_{i-1} = Up(\overline{L}_i)$, $\{i = 4, 3, 2\}$, $Up()$ denotes the linear interpolation of the up sampling operation. Finally, input G_{i-1} and L_{i-1} into the MAWF yields the weighted feature, putting weighted feature into the CPCM to get feature $\overline{L}_{i-1}$. This process can be described as $\overline{L}_{i-1} = C(M(G_{i-1}, L_{i-1}))$, $\{i = 4, 3, 2\}$, $M()$ and $C()$ representing the data pass through the MAWF and CPCM, respectively. $\overline{L}_{i-1}$ is used as the fully local feature inputs for the next weighted fusion and convolution point-wise modules.

3.1 | Maximum-average pooling weighted of feature fusion modules (MAFM)

Works such as in Refs. [26, 27] have demonstrated that not all channel features play an equally important role in model expressiveness. Therefore, strengthening the features of important channels and weakening the features of unimportant channels will help the model representation.

To better strengthen the features of important channels of global features $G\{G_1,G_2,G_3,G_4\}$ *and* local features $L\{L_1, L_2, L_3,L_4\}$as well as to weaken the features of their unimportant channels, this paper proposed a maximum-average pooling weighting module, and the structure shown in Figure 3. The MAFM module performs the following process for global and local features.

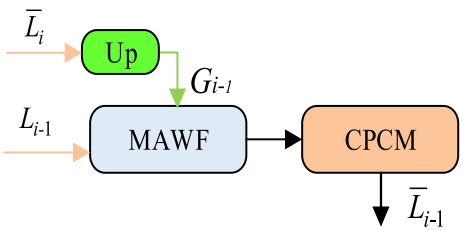

FIGURE 2 Maximum-average pooling weighted fusion module and point-wise convolution module (MAWF + CPCM).

1. The global feature G and the local feature L are both subjected to the maximum pooling operation, and we get the feature of size $c \times 1 \times 1$. The maximum pooling operation is given in Equation (1).

$$\mathrm{Amp}_c(p) = \max(p) \tag{1}$$

Amp() denotes the maximum pooling operation, and $p \in R^{c\times w\times h}$ is the input feature. Then, they are multiplied by the corresponding global feature G and local feature L, respectively, to obtain the corresponding global maximum weighted feature $G_m \in R^{c\times w\times h}$ and local maximum weighted feature $L_m \in R^{c\times w\times h}$. Adding the two features to get the weighted maximum pooling feature, we obtained formula which is given in Equation (2).

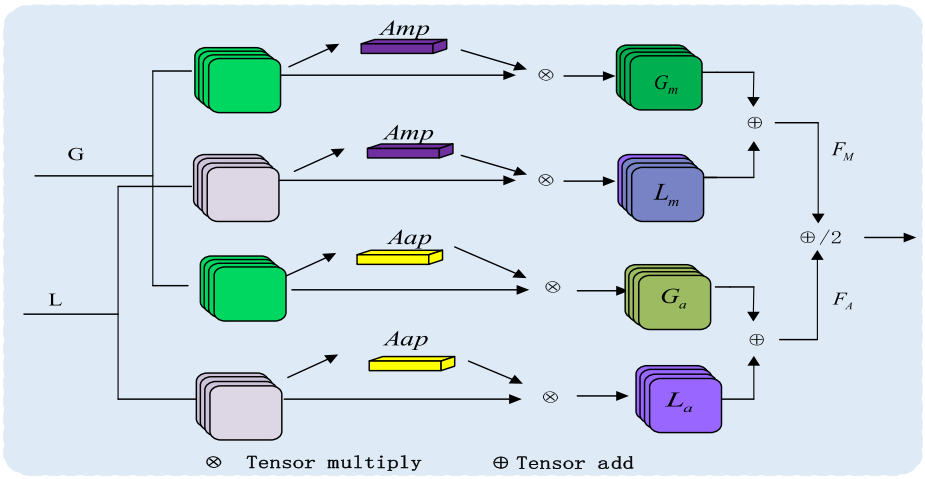

FIGURE 3 Maximum-average pooling weighted of feature fusion modules.

$$F_m = \underbrace{\mathrm{Amp}(G) \times G}_{G_m} + \underbrace{\mathrm{Amp}(L) \times L}_{L_m} \tag{2}$$

2. The global feature G and local feature L are both subjected to the averaging pooling operation, which yields a feature of size $c \times 1 \times 1$, and the averaging pooling operation is shown in Equation (3).

$$\mathrm{Aap}_c(p) = \frac{1}{w \times h} \sum_{i=0}^{w} \sum_{j=0}^{h} p_{ij} \tag{3}$$

Aap() denotes the averaging pooling operation, w and h are the height and width of the input feature $p \in R^{c \times w \times h}$ respectively.

Then, they are multiplied by the corresponding global feature G and local feature L, respectively, to get the corresponding global average pooling feature G_a and the local average pooling feature L_a. Feature G_a and feature L_a are added to obtain the weighted average pooling feature. The calculation formula is given in Equation (4).

$$F_a = \underbrace{\mathrm{Aap}(G) \times G}_{G_a} + \underbrace{\mathrm{Aap}(L) \times L}_{L_a} \tag{4}$$

Finally, the weighted maximum pooling feature F_m and the weighted average pooling feature F_a are averaged to get the features of size $c \times w \times h$ as the output of the module.

In this module, both global and local features are subjected to maximum pooling and average pooling weighting, the two results were summed to take the average value. The input feature after dealing with maximum pooling or average pooling, the result is the weighted weight value for each channel of the input features. The feature information of the channel is important if the weight value is large. Otherwise, the feature information of the channel is not important. The weight operation is completed by multiplying the weighted value and the corresponding feature. The advantage of this series of weighting operations is that the MAFM module has a strong filtering mechanism and enhancement mechanism. It can adaptively filter irrelevant feature information, eliminate redundant information and enhance useful. Therefore, it contributes to refine global and local feature information, improves the decoding capacity of the decoder and compensates image detail information.

3.2 | Continuous point-wise convolution modules (CPCM)

A common practice to reduce the parameters of the network model is to reduce the number of convolution layers or to use smaller convolution kernels. However, reducing the number of network layers may lead to extract feature insufficiently, and using small convolution kernels cause small network perceptual fields problem, which in turn leads to problems such as narrower features in the interrogation region and poorer global features obtained. To solve the above problem, we design a continuous point-wise convolution module (CPCM), as shown in Figure 4, which is stitched together by three identical sub-modules (Block1, Block2 and Block3). Each sub-module consists of three convolution layers, sub-module with input feature channels c_1 larger than the output c_2, the output feature channels of the three convolution layers are $\frac{c_2}{2}$, $\frac{c_2}{2}$ and c_2, detailed structure and parameters are shown in the dashed box in Figure 4. For example, when the input feature size is $64 \times w \times h$, the output size is $32 \times w \times h$, the number of parameters for convolution with only one layer of 3×3 convolution kernels is 18,432, while the number of parameters for one block of CPCM module is 3712, which is only 20% of the number of parameters of the former. In the process of data flow to the CPCM modules, 1×1 small convolution kernel and 3×3 large convolution kernel are used at intervals. 1×1 convolution kernel can greatly reduce the feature channel, while 3×3 convolution kernel retains a larger receptive fields, and the use of multiple 3×3 convolution kernels is equivalent to using a larger convolution kernel, which provides a broader

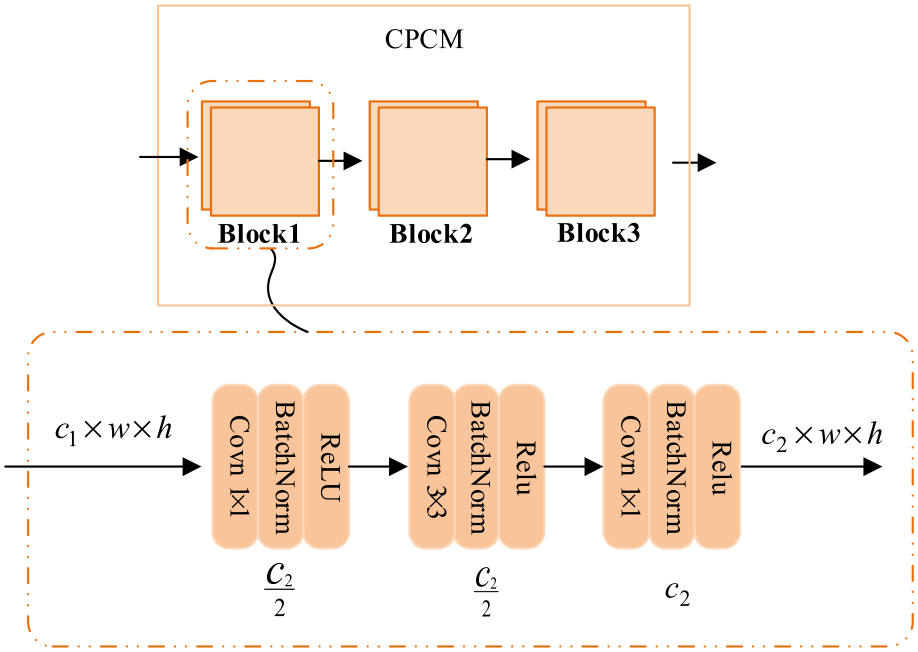

FIGURE 4 Continuous pointwise convolution module.

receptive field for the model. It means that the model can also detect depth information globally and avoid the problem of inaccurate depth information estimation.

4 | EXPERIMENT

4.1 | Dataset

KITTI: This is one of the most important test sets in the field of autonomous driving at present. The resolution of the images in this dataset is 1224 × 368. We train our network using approximately 11,000 images on a random crop of 1216 × 352 and test on 357 images.

NYU Depth V2: This is a dataset of various indoor scene images and corresponding depth maps obtained by the Microsoft Kinect camera, which is the most widely used for the task of single-view depth prediction. The images in this dataset have a resolution of 640 × 480. We crop the images to their centre to obtain images of size 576 × 448. We use 24,000 pairs of these images to train our network and test it on 654 images.

4.2 | Data preprocessing

We use a depth data enhancement method [28] to handle the dataset, which replaces part of the input RGB image with a true depth map to provide diversity in the input image as well as enable the network to focus on high frequency regions. To avoid aoverfitting while training the module, we also use flip, brightness, random gamma transform, hue saturation value methods for data enhancement. Depth information range mapping for studying the range of depth estimation of this method is used.

- Flip: Both the monocular colour image and the corresponding depth image are flipped horizontally with 50% probability
- Brightness Contrast: increase the virtual variation of the input image by randomly increasing or decreasing the brightness of the image, and the limit range of both brightness and contrast is [−0.2, 0.2].
- Random Gamma Transform: Gamma transform is performed on colour images and depth images, and the parameter range is [80, 100].
- Hue Saturation Value: Enhance the hue saturation value of the image.
- Depth information range mapping: Map the NYUDepthV2 depth information range to within 10 m, and map the KITTI depth information range to within 80 m.

4.3 | Implementation detail

To compute the distance between the predicted output y* and the ground truth depth map y, we use a scale-invariant log-scale loss to train the model that forms the work in Ref. [29]. The calculation formula of the training loss is shown in Equation (5).

$$\text{loss} = \frac{1}{n}\sum_{i=0} d_i^2 + \frac{1}{2n^2}\sum_{i=0} d_i^2 \tag{5}$$

Where $d_i = \log y_i + \log y_i^*$.

The encoder module in the network is initialised by the pretrained weights of the SegFormer model. The initialisation of the network parameters of the non-encoder part is random. We use the Adam optimiser with training epochs of 25 epochs. The initial learning rate is 0.0001 and is reduced to 10% every five epochs. We set $\beta_1 = 0.9, \beta_2 = 0.999$ and use a weight decay of 0.0001. The experiments are carried out on the NVIDIA Tesla T4 16G GPU platform and PyTorch framework.

4.4 | Evaluation

In this study, we use five metrics provided in Ref. [5] to evaluate the accuracy of model depth information estimation. The five metrics are the Mean Relative Error (REL), Mean Square Error (RMS), Mean Log Error (log10), Accuracy under threshold $t_d : \max\left(d_i^*/d_i, d_i/d_i^*\right)$ and Logarithmic Root Mean Square Error (RMSElog). The specific formulae for the five evaluation metrics are as follows Equation (6) (7) (8) (9) (10).

$$\mathrm{REL} = \frac{1}{N}\sum_{i=0}^{N}\frac{\left|d_i - d_i^*\right|}{d_i^*} \tag{6}$$

$$\mathrm{RMS} = \sqrt{\frac{1}{N}\sum_{i=0}^{N} d_i - d_i^*} \tag{7}$$

$$\log 10 = \frac{1}{N}\sum_{i=0}^{N}\left|\lg d_i - \lg d_i^*\right| \tag{8}$$

$$\max\left(\frac{d_i^*}{d_i}, \frac{d_i}{d_i^*}\right) = \sigma < t_d\left(t_d \in \left[1.25^1, 1.25^1, 1.25^1\right]\right) \tag{9}$$

$$\mathrm{RMSElog} = \sqrt{\frac{1}{N}\sum_{i=0}^{N}\left|\lg d_i - \lg d_i^*\right|} \tag{10}$$

where N denotes the total number of pixels in the depth image, denotes the i th pixel on the predicted depth, and denotes the ith pixel on the true depth image.

4.5 | Experimental results and analysis

4.5.1 | Comparison with state of the arts

A comparison of the proposed method and some recent state-of-the-art methods on the KITTI dataset, as shown in Table 1. Params(M) is the number of model parameters, and the third column is the pixel-level accuracy of the predicted depth maps at a threshold value 1.25^1,1.25^2,1.25^3, respectively, and their larger values represent better performance. The metrics in the fourth column are REL, RMS and RMSElog10, and the smaller the values are the better the performance. As can be seen from the table, our proposed methods achieve the advanced performance in six metrics on the KITTI Dataset. Kim et al. [6] used select features to build lightweight decoders leads to shallow decoder layers and insufficient progress in

TABLE 1 Accuracy evaluation of different methods tested on KITTI dataset.

		Higher is better (δ<) ↑			Lower is better ↓		
Method	**Params(M)**	**1.25^1**	**1.25^2**	**1.25^3**	**REL**	**RMS**	**RMSElog**
Yin et al. [16]	114	0.938	0.984	0.998	0.072	3.258	0.117
Bhat et al. [17]	78	0.903	0.988	0.997	0.062	2.573	0.092
Ranftl et al. [18]	122	0.959	0.955	0.999	0.058	2.360	0.088
Kim et al. [6]	62	0.967	0.955	0.999	0.057	2.297	0.086
Li et al. [19]	-	0.975	0.997	0.999	0.058	2.143	0.088
Ours	60	**0.996**	**0.999**	**0.999**	**0.056**	**2.015**	**0.081**

Note: Bold numbers indicate best performance.

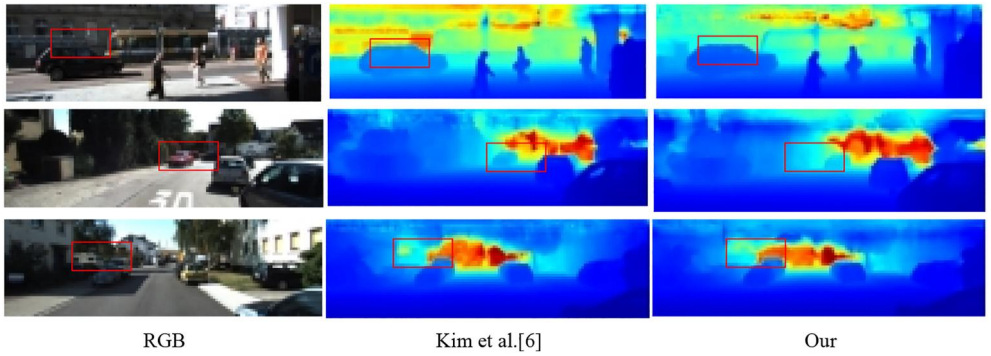

FIGURE 5 The test results of several models tested in four different outdoor scenes on the KITTI dataset. The contrast of the edges in the red box is obvious.

depth estimation in the face of complex and variable outdoor environments. In Ref. [18], two encoder branches are used for feature extraction of RGB images, which can extract rich image features, but different encoders perceive feature types differently, which makes the feature decoding work difficult in the later stage. Our method uses only one encoder, Feature fusion, by strengthening important channel features and weakening unimportant channels to improve the depth estimation accuracy. In comparison with recent advanced methods, we have the lowest number of model parameters, only about 60 million parameters. The reason is we design the point-wise convolution module to work with the maximum-average pooling weighted fusion module, and it can compress the channels of input, thus reducing the number of model parameters.

We compare scenes collected on the KITTI dataset for different time periods and road segments, and the results are shown in Figure 5. Both our methods and the methods [6] provide predictions out of reasonable depth image vision, but our estimated depth maps reveal more details and are more

TABLE 2 Accuracy evaluation of different methods tested on the NYU Depth V2 dataset.

		Higher is better (δ<) ↑			Lower is better ↓		
Method	**Params(M)**	**1.25^1**	**1.25^2**	**1.25^3**	**REL**	**RMS**	**RMSElog**
Chen et al. [3]	-	0.853	0.959	0.991	0.121	0.545	0.052
Ramamon et al. [22]	-	0.888	0.979	0.995	0.139	0.495	0.047
Yin et al. [16]	-	0.875	0.976	0.994	0.108	0.416	0.048
Swami et al. [4]	-	0.870	0.974	0.993	0.115	0.528	0.049
Hu et al. [5]	68	0.843	0.968	0.991	0.126	0.555	0.054
Xue et al. [9]	220	0.846	0.969	0.992	0.123	0.550	0.053
Bhat et al. [17]	78	0.903	0.988	0.997	0.103	0.364	0.044
Ranftl et al. [18]	123	0.904	0.988	0.997	0.110	0.357	0.045
Kim et al. [6]	62	**0.915**	**0.998**	0.997	0.098	0.344	0.042
Ours	**60**	0.912	0.986	**0.998**	**0.098**	**0.334**	0.043

Note: Bold numbers indicate best performance.

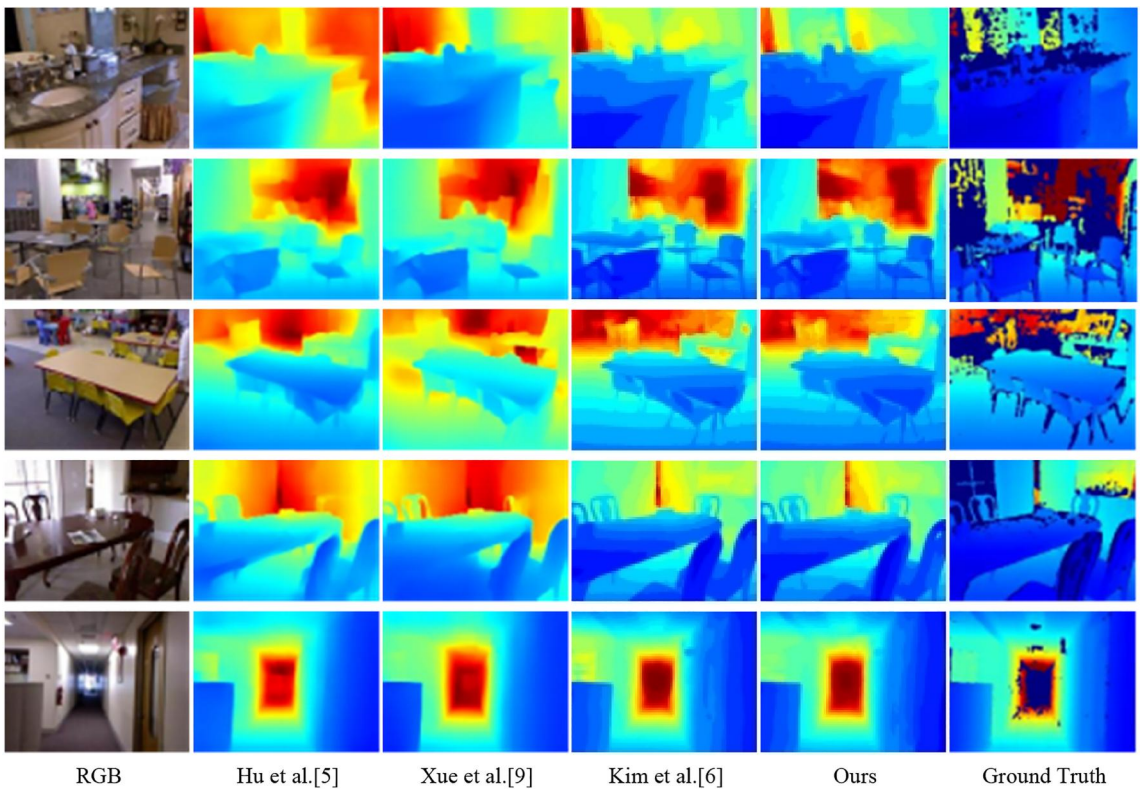

FIGURE 6 Visualise the results of different methods on five different indoor scenes on the NYU Depth V2 dataset.

accurate near object boundaries. For example, depth information of pedestrian is more complete, and the car has the most accurate contour. This shows that our proposed feature fusion scheme is effective in estimating depth information accurately.

Table 2 shows the comparison between our proposed method and some recent state-of-the-art methods on the NYU Depth v2 dataset. As can be seen from the table, the number of parameters of our proposed model is 60M, which is the smallest among all the models. Three of the six metrics achieve good performance, and the remaining three are close to the best performance in recent years. In the works [5, 9], they use Sobel operator edge detection to induce boundary information generation, which leads their methods to focus on the boundary information and ignore the overall depth information, resulting in insufficient accuracy of depth information estimation. Our methods effectively avoid the problem that depth information estimation with edge-induced in the works [5, 9] by strengthening the features of important channels and weakening the features of non-important channels.

Figure 6 shows the tests of different methods on five different indoor scenes (restroom, bookstore, classroom and restaurant office) of NYU Depth V2 dataset. The visual results show that our method has a stronger prediction capacity in dealing with indoor scenes with complex objects, abrupt changes in depth information and various lighting conditions. The depth images predicted by our method are more detailed than the works in Refs. [5, 6, 9], for example, the outline of a table and chair is more clear.

In order to prove the generalisation capacity of our model, the dataset in another room is designed to test the model that has completed training on the NYU Depth v2 dataset. The

TABLE 3 Accuracy evaluation of different methods tested on the iBims-1 dataset.

		Higher is better (δ<) ↑			Lower is better ↓		
Method	**Params(M)**	**1.25^1**	**1.25^2**	**1.25^3**	**REL**	**RMS**	**Log10**
Chen et al. [3]	-	0.51	0.84	0.94	0.22	1.14	0.11
Ramamon et al. [22]	-	0.59	0.84	0.94	0.26	1.06	0.11
Yin et al. [16]	-	0.54	0.84	0.93	0.24	1.06	0.11
Swami et al. [4]	-	0.60	0.87	0.95	0.20	1.03	0.10
Hu et al. [5]	68	0.52	0.85	0.95	0.23	1.13	0.12
Xue et al. [9]	220	0.51	0.82	0.93	0.24	1.19	0.12
Bhat et al. [17]	78	0.55	0.86	0.95	0.22	1.07	0.11
Ranftl et al. [18]	123	0.56	0.86	0.95	0.23	1.13	0.12
Kim et al. [6]	62	**0.61**	**0.89**	0.96	**0.20**	1.01	0.10
Ours	**60**	0.60	0.88	**0.96**	0.21	**1.01**	**0.10**

Note: Bold numbers indicate best performance.

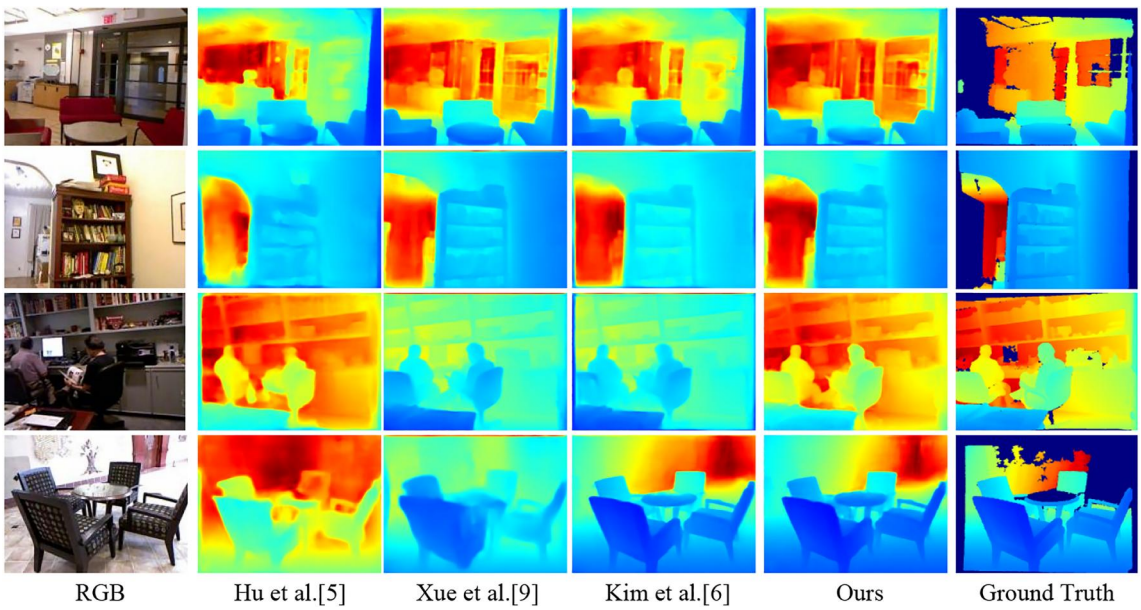

FIGURE 7 Visualise the results of different methods on four different indoor scenes on the SUN-RGBD dataset.

TABLE 4 Test results of our method on NYU Depth V2 and KITTI with and without the use of the average-maximum pooling weighting module, respectively.

Dataset		Higher is better (δ<) ↑			Lower is better ↓			
		1.25^1	1.25^2	1.25^3	REL	RMS	RMSElog	Log10
NYU depth V2	Ours*	0.901	0.977	0.994	0.112	0.351	-	0.52
	Ours	**0.912**	**0.986**	**0.998**	**0.099**	**0.344**	-	**0.041**
KITTI	Ours*	0.985	0.998	0.998	0.075	2.255	0.088	-
	Ours	**0.996**	**0.999**	**0.999**	**0.056**	**2.015**	**0.081**	-

Note: Bold numbers indicate best performance. * indicates that the MAWF module is not used.

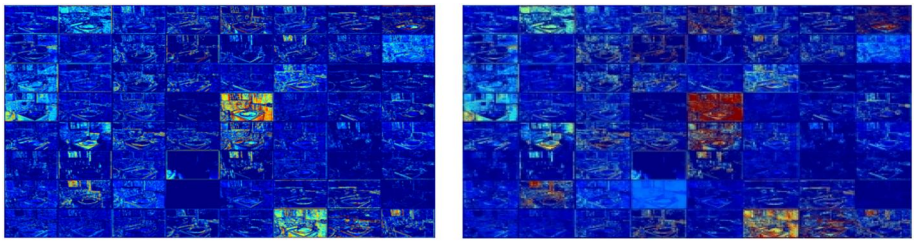

FIGURE 8 Visualisation of weighted operation using max pooling.

iBims-1 dataset [30] is an RGB-D dataset obtained by digital single-lens reflection (DSLR) camera and high-precision laser scanner. It contains various indoor high-quality deep images and a high-resolution RGB image. The data distribution is completely different from NYU Depth v2. A hundred pairs of the iBims-1 dataset are used for evaluation. The test results are shown in Table 3. Our method achieves three indicators' best performance. We qualitatively analyse our method on another SUN-RGBD indoor dataset [31] to show its generalisation performance, as shown in Figure 7. The results of the methods in literature [5, 6, 9] are blurred to varying degrees, while the depth image of the method in this study is clear, and the three-dimensional structure is reasonable. This fully shows that the method in this study has strong depth estimation capacity in various indoor environments, therefore, the model generalisation capacity is strong.

TABLE 5 Results for the NUY Depth V2 dataset mapped to each of the 8 depth-of-field ranges.

Depth range (m)	Higher is better (δ<) ↑			Lower is better ↓		
	1.25^1	1.25^2	1.25^3	REL	RMS	Log10
0~10 m	**0.912**	**0.986**	**0.998**	**0.099**	**0.344**	**0.043**
0~20 m	0.910	0.986	0.996	0.101	0.704	0.042
0~30 m	0.908	0.986	0.997	0.101	1.055	0.042
0~40 m	0.908	0.985	0.995	0.102	1.423	0.043
0~50 m	0.907	0.986	0.995	0.104	1.706	0.044
0~60 m	0.903	0.985	0.995	0.102	2.143	0.045
0~70 m	0.905	0.985	0.995	0.101	2.469	0.044
0 ~80 m	0.910	0.985	0.995	0.098	2.816	0.042

Note: Bold numbers indicate best performance.

4.5.2 | Ablation experiments

1) Visualisation of average-maximum pooling weighting module

In order to verify whether our maximum-average pooled weighted feature fusion module has a helpful effect on the prediction of depth information, we also performed ablation experiments. We put the global features and local features only for channel concat operation instead of the operation of the weighting module part in the average-maximum pooling weighting module and conducted separate experiments on NYU Depth V2 and KITTI, and the test results are shown in Table 4. Figure 8 shows the comparison before and after using maximum pooling weighting methods in the MAMF. The left side of Figure 8 shows the visualisation of the feature map before weighting, and the right side of Figure 8 shows the visualisation of the feature map after weighting. The plot on the right is darker and has more texture detail information than the left one.

Table 4 shows that the six results on NYU Depth V2 and KITTI are improved after using the maximum-average pooling weighting module. The reason is that channels concat operation will fuse the extraneous information of depth estimation and increase the burden of the model on the decoding of depth information. But, the MAFM module is used to fuse features that can strengthen the features of important channels and weaken the features of unimportant channels. Therefore, it can improve the deep information decode capacity of the model effectively.

2) Different depth-of-field range experiments

Different cameras capture different depth-of-field ranges. To verify our proposed method that can adapt to different ranges of depth-of-field scenes, in this subsection, we train the NUY Depth V2 dataset after depth information mapped eight ranges, and the results are shown in Table 5. Our method has better performance in all eight depth-of-field ranges, with the best performance in the range of 0–10 m.

TABLE 6 Results of edge information tested by different methods on NYU Depth V2 datasets.

Threh	Method	Precision ↑	Recall↑	F1-score↑
>0.25	Fu et al. [21]	0.320	0.583	0.402
	Hu et al. [5]	0.635	0.480	0.540
	Xue et al. [9]	**0.644**	0.483	0.546
	Kim et al. [6]	0.515	0.636	0.554
	Ours	0.503	**0.639**	**0.549**
>0.5	Fu et al. [21]	0.316	0.473	0.412
	Hu et al. [5]	0.664	0.476	0.547
	Xue et al. [9]	0.665	0.492	**0.558**
	Kim et al. [6]	0.675	0.449	0.526
	Ours	**0.676**	**0.513**	0.517
>1	Fu et al. [21]	0.483	0.512	0.485
	Hu et al. [5]	0.755	0.514	0.604
	Xue et al. [9]	0.750	**0.531**	**0.613**
	Kim et al. [6]	0.776	0.315	0.439
	Ours	**0.780**	0.343	0.440

Note: Bold fonts represent the best performance.

4.5.3 | Comparison of scene edge accuracy

To better demonstrate that the module we designed has a strong performance enhancement for the whole network, we evaluate the prediction capacity of our model on the edge information of the image scene that follow evaluation indicator of the works [5], and Table 6 shows the comparison of the edge information restoration capacity of our method with the advanced methods on the NYU Depth V2 dataset. Works in Ref. [5]output the depth image of size is 152 × 114, and our output is 576 × 448. To compare the performance more fairly, we resize the output depth image to 152 × 114 size before evaluation. From the data in Table 6, two of the three metrics (Precision, Recall, and F1-score) of our method are ahead of other methods when the threshold (Threh) is greater than 0.25 and greater than 0.5, and one of the metric is ahead of other methods when the Threh is greater than one. Our model as well as Ref. [6] outputs depth images with higher resolution and richer depth information.

4.5.4 | Robustness experiments

The robustness of the model for depth estimation is critical because sometimes the images taken by the camera may be noisy or blurred in rainy or foggy weather. In this subsection, we do not retrain the network with the noisy dataset but use the trained network model from the original NYU Depth V2 dataset for robustness experiments. The trained network model is tested by processing the input with Gaussian Noise, Motion Blur and Contrast methods in the test set RGB images of NYU Depth V2, respectively, and the test results are shown in Table 7.

As can be seen in Table 7, our method still has a strong depth estimation capacity for RGB images processed using Gaussian Noise, Motion Blur and Contrast. Compared with

TABLE 7 Experimental results of testing robustness of different models on NYU Depth V2 dataset.

		Higher is better (δ<) ↑			Lower is better ↓		
Corruption type	Method	1.25^2	1.25^3	1.25^2	REL	RMS	RMSElog
Gaussian noise	Lee et al. [23]	0.223	0.384	0.543	0.435	1.589	0.743
	Bhat et al. [17]	0.347	0.553	0.708	0.343	1.299	0.544
	Kim et al. [6]	0.775	0.940	0.983	0.161	0.541	0.198
	Ours	**0.909**	**0.987**	**0.997**	**0.099**	**0.353**	**0.125**
Motion blur	Lee et al. [23]	0.677	0.850	0.922	0.189	0.701	0.279
	Bhat et al. [17]	0.697	0.859	0.927	0.180	0.643	0.262
	Kim et al. [6]	0.807	0.946	0.981	0.139	0.494	0.183
	Ours	**0.909**	**0.985**	**0.997**	**0.101**	**0.354**	**0.126**
Contrast	Lee et al. [23]	0.697	0.864	0.932	0.181	0.198	0.689
	Bhat et al. [17]	0.654	0.836	0.917	0.198	0.234	0.752
	Kim et al. [6]	0.860	0.971	0.992	0.117	0.074	0.427
	Ours	**0.912**	**0.986**	**0.977**	**0.099**	**0.350**	**0.124**

Note: Bold fonts represent the best performance.

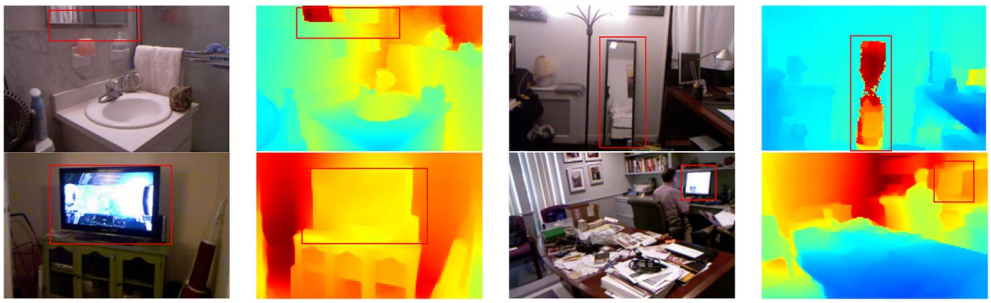

FIGURE 9 Limitations of the methodology in this paper.

methods in the works [6, 17, 23], all six evaluation metrics of our model are optimal, which shows that our model is more robust; the reason is that the maximum-average pooling weighted fusion module is used that can filter noise, blur and other information. Some unimportant feature information is weakened to avoid the model learn useless information.

4.5.5 | Limitations analysis

Although the method in this study has achieved excellent performance, there are still limitations, for example, when there is a TV screen or mirror in the scene, the depth of the region and its surrounding areas are not estimated accurately, as shown in Figure 9. The objects in the red box are mirrors or televisions, the TV screen and mirror make the model misunderstand the scene information and give wrong results. Later work will focus on improving these problems.

5 | CONCLUSION

This paper proposes a depth estimation method based on weighted fusion and point-wise convolution. We design a maximum-average adaptive pooling weighted fusion module (MAWF) that fuses global features and local features and a continuous point-wise convolution module (CPCM) for processing the fused features derived from the (MAWF) module and reducing the number of network model parameters, which can better decode the depth information of a scene. Experimental results show that our method achieves state-of-the-art performance on KITTI dataset. The experiments on NUY Depth V2 dataset show that the method can estimate the depth of different depth ranges and has strong robustness. The quantitative analysis of iBims-1 dataset and the qualitative analysis of SUN-RGBD dataset show that the method has strong generalisation capacity. However, the method in this study has problems of inaccurate area estimation in scenes on TV and in mirrors. Later work will focus on improving these problems.

AUTHOR CONTRIBUTIONS

Conceptualisation: Ideas; formulation or evolution of overarching research goals and aims. Methodology: Development or design of methodology of depth estimation; creation of models. Software: Programming; designing computer programmes; implementation of the computer code and supporting algorithms. Formal analysis: computational, or other formal techniques to analyse or synthesise study data. Paper writing: Writing of paper manuscripts.

ACKNOWLEDGEMENT

National Natural Science Foundation of China (Fund No: 61763002).

CONFLICT OF INTEREST STATEMENT

We declare that we do not have any commercial or associative interest that represents a conflict of interest in connection with the work submitted.

PERMISSION TO REPRODUCE MATERIALS FROM OTHER SOURCES

None.

DATA AVAILABILITY STATEMENT

Data derived from public domain resources. These data were derived from the following resources available in the public domain: KITTI: https://www.cvlibs.net/datasets/kitti/user_login.php NYU Depth V2: https://cs.nyu.edu/~silberman/datasets/nyu_depth_v2.html iBims −1: https://dataserv.ub.tum.de/index.php/s/m1455541 SUN-RGB-D: https://rgbd.cs.princeton.edu/data/.

ORCID

Chen Lei https://orcid.org/0000-0003-1850-7507

REFERENCES

1. Zhou, T., et al.: Unsupervised learning of depth and ego-motion from video. In: Proceedings of the IEEE Conference on Computer Vision and Pattern Recognition, pp. 1851–1858 (2017)
2. Yin, Z., Shi, J.: Geonet: unsupervised learning of dense depth, optical flow and camera pose. In: Proceedings of the IEEE Conference on Computer Vision and Pattern Recognition, pp. 1983–1992 (2018)
3. Chen, X., Chen, X., Zha, Z.-J.: Structure-aware residual pyramid network for monocular depth estimation. arXiv preprint arXiv:1907.06023 (2019)
4. Swami, K., Bondada, P.V., Bajpai, P.K.: Aced: accurate and edge-consistent monocular depth estimation. In: 2020 IEEE International Conference on Image Processing (ICIP), pp. 1376–1380. IEEE (2020)
5. Hu, J., et al.: Revisiting single image depth estimation: toward higher resolution maps with accurate object boundaries. In: 2019 IEEE Winter

Conference on Applications of Computer Vision (WACV), pp. 1043–1051. IEEE (2019)
6. Kim, D., et al.: Global-local path networks for monocular depth estimation with vertical CutDepth. arXiv preprint arXiv, pp. 2201–07436 (2021)
7. Silberman, N., et al.: Indoor segmentation and support inference from rgbd images. In: European Conference on Computer Vision. Springer, Berlin (2012)
8. Geiger, A., Lenz, P., Urtasun, R.: Are we ready for autonomous driving? The kitti vision benchmark suite. In: 2012 IEEE Conference on Computer Vision and Pattern Recognition. IEEE (2012)
9. Xue, F., et al.: Boundary-induced and scene-aggregated network for monocular depth prediction. arXiv preprint arXiv, pp. 2102–13258 (2021)
10. Huynh, L., et al.: Guiding monocular depth estimation using depth-attention volume. In: European Conference on Computer Vision, pp. 581–597. Springer, Cham (2020)
11. Yang, X., et al.: Monocular depth estimation with sharp boundary. In: 2022 8th International Conference on Virtual Reality (ICVR), pp. 384–391. IEEE (2022)
12. Liu, J., et al.: Multi-scale residual pyramid attention network for monocular depth estimation. In: 2020 25th International Conference on Pattern Recognition (ICPR), pp. 5137–5144. IEEE (2021)
13. Dong, X., et al.: Mobilexnet: an efficient convolutional neural network for monocular depth estimation. IEEE Trans. Intell. Transport. Syst. 23(11), 20134–20147 (2022). https://doi.org/10.1109/tits.2022.3179365
14. Wang, L., et al.: Sdc-depth: semantic divide-and-conquer network for monocular depth estimation. In: Proceedings of the IEEE/CVF Conference on Computer Vision and Pattern Recognition, pp. 541–550 (2020)
15. Eigen, D., Fergus, R.: Predicting depth, surface normals and semantic labels with a common multi-scale convolutional architecture. In: Proceedings of the IEEE International Conference on Computer Vision, pp. 2650–2658 (2015)
16. Yin, W., et al.: Enforcing geometric constraints of virtual normal for depth prediction. In: Proceedings of the IEEE/CVF International Conference on Computer Vision, pp. 5684–5693 (2019)
17. Bhat, S.F., Alhashim, I., Peter, W.: 'Adabins: depth estimation using adaptive bins. In: Proceedings of the IEEE/CVF Conference on Computer Vision and Pattern Recognition, pp. 4009–4018 (2021)
18. Ranftl, R., Bochkovskiy, A., Koltun, V.: Vision transformers for dense prediction. In: Proceedings of the IEEE/CVF International Conference on Computer Vision (2021)
19. Li, Z., et al.: DepthFormer: exploiting long-range correlation and local information for accurate monocular depth estimation. arXiv preprint arXiv, pp. 2203–14211 (2022)
20. Vaswani, A., et al.: Attention is all you need. Adv. Neural Inf. Process. Syst. 30 (2017)
21. Fu, H., et al.: Deep ordinal regression network for monocular depth estimation. In: CVPR. (2018)
22. Ramamonjisoa, M., and Vincent, L.: Sharpnet: fast and accurate recovery of occluding contours in monocular depth estimation. In: Proceedings of the IEEE/CVF International Conference on Computer Vision Workshops (2019)
23. Lee, J.H., et al.: From big to small: multi-scale local planar guidance for monocular depth estimation. arXiv preprint arXiv:1907.10326 (2019)
24. Xie, E., et al.: SegFormer: simple and efficient design for semantic segmentation with transformers. Adv. Neural Inf. Process. Syst., 12077–12090 (2021)
25. Dosovitskiy, A., et al.: An image is worth 16x16 words: transformers for image recognition at scale. arXiv preprint arXiv:2010.11929 (2020)
26. Hu, J., Shen, Li, Sun, G.: Squeeze-and-excitation networks. In: Proceedings of the IEEE Conference on Computer Vision and Pattern Recognition, pp. 7132–7141 (2018)
27. Woo, S., et al.: Cbam: convolutional block attention module. In: Proceedings of the European Conference on Computer Vision (ECCV), pp. 3–19 (2018)
28. Ishii, Y., and Yamashita, T.: CutDepth: edge-aware data augmentation in depth estimation. arXiv preprint arXiv:2107.07684 (2021)
29. Eigen, D., Puhrsch, C., Fergus, R.: Depth map prediction from a single image using a multi-scale deep network. Adv. Neural Inf. Process. Syst. 27 (2014)
30. Koch, T., et al.: Evaluation of cnn-based single-image depth estimation methods. In: Proceedings of the European Conference on Computer Vision (ECCV) Workshops (2018)
31. Song, S., Lichtenberg, S.P., Xiao, J.: Sun rgb-d: a rgb-d scene understanding benchmark suite. In: CVPR (2015)

How to cite this article: Lei, C., Zhengyou, L., Yu, S.: A monocular image depth estimation method based on weighted fusion and point-wise convolution. IET Comput. Vis. 17(8), 1005–1016 (2023). https://doi.org/10.1049/cvi2.12212